EFFICIENT MODELING OF UNSTEADY CONTROL SURFACE AERODYNAMICS IN TRANSONIC FLOW FOR FLIGHT DYNAMICS ANALYSIS OF THE INTELLIGENT WING

L.-H. Lemke*, K. Krall*, F. Thielecke*, J. Müller†

* Hamburg University of Technology, Institute of Aircraft Systems Engineering, Nesspriel 5, 21129 Hamburg, Germany

† University of Stuttgart, Institute of Aerodynamics and Gas Dynamics, Pfaffenwaldring 21, 70569 Stuttgart, Germany

Abstract

The *Intelligent Wing* is a research concept of a multifunctional wing combining classical functions as high-lift, lift dumping and roll control, with newer functions as structural loads control, structural health monitoring or flutter suppression. Therefore, the intelligent wing uses a high number of dynamic control surfaces. In particular for the design of active maneuver and gust load control functions and their evaluation, the unsteady aerodynamic effect of dynamic control surface deflections play a major role. For transport aircraft in transonic flight, this is especially true, as the phase shift between the control surface deflection and the aerodynamic effect due to the translational movement of shock waves significantly influences the controller design and its overall potential for load reduction. In this paper, an efficient model structure is proposed with which the unsteady aerodynamic effect of dynamic control surface deflections can be predicted. This method enables fast simulations in the time domain of a flight dynamics model with multiple dynamic control surfaces on the wings.

Keywords

Control Surface Aerodynamics; Unsteady Aerodynamics; Intelligent Wing

1. INTRODUCTION

The *Intelligent Wing* is a research concept of a multifunctional wing combining classical functions as high-lift, lift dumping and roll control, with newer functions as structural loads control, structural health monitoring or flutter suppression.

Load control functions promise a lower structural weight and enable a higher wing aspect ratio due to reduced design loads. On the other hand, these load control functions require fast control surface deflections, especially in high-speed flight through wind gusts, which leads to challenging requirements for the actuation system. The evaluation of the overall potential of load control functions and their integration into a practicable wing concept is part of the investigations concerning the *Intelligent Wing*.

In order to evaluate the overall potential of load control functions, multidisciplinary simulations of gust encounters and maneuver flights are required. These simulations must include the disciplines aerodynamics, structural dynamics, actuation system dynamics and the controller functions to cover all significant effectors. Additionally, the simulation must be able to predict the unsteady load distribution of the wing in order to evaluate the holistic load reduction.

Due to the many different disciplines included in the simulation and the high number of simulations necessary to compare different control laws and strategies in various scenarios, the computation effort is a major design variable for the model. Therefore, in this paper a model structure is proposed by which the unsteady distributed aerodynamic effect of multiple dynamically deflected control surfaces can be predicted efficiently. Common techniques for the aerodynamic modeling of unsteady control surfaces use either a Doublet-Lattice Method (DLM) in addition with corrections for nonlinear effects, or Computational Fluid Dynamics (CFD) programs, e.g. based on Navier-Stokes analysis [1] [2]. Not only does the DLM approach need many corrections and a transfer from frequency domain to the time domain, e.g. via a rational function approximation, but it also leads to inaccurate results for unsteady transonic conditions [1]. Furthermore, the computation effort for CFD analysis is quite high, such that an efficient usage for a broad evaluation of several controllers in various scenarios is not feasible. In 2021, Lancelot et al. published a method for the modeling of unsteady control surface deflections using simple lookup tables and transfer functions determined by few CFD analysis [3]. Thereby, the total effect of the dynamic control surface deflection is divided into a steady portion and an unsteady part. The nonlinear steady effect is calculated by lookup tables, determined by steady CFD analysis of con-

doi: 10.25967/610033

stant deflection angles. For the determination of the transfer function, an unsteady CFD analysis of a dynamic deflection is compared to the steady solution calculated with the lookup table. Lastly, using this method, the total distributed aerodynamic effect of an arbitrary dynamic control surface deflection can be calculated with an accuracy in the range of CFD analysis plus $5\,\%$ error for most cases [3]. The total number of lookup tables and transfer functions necessary for this approach depend on the number of points to discretize the aerodynamic distribution, the number of aerodynamic coefficients of interest and the number of control surfaces. While the method works well for aircraft configurations with few control surfaces, the model for the here considered configuration with multiple individual control surfaces per wing would lead to an excessive modeling effort. Therefore, an improved method regarding the efficiency, which is based on this approach by Lancelot et al., is presented in the following.
In section 2, a flight dynamics base model and the here used reference aircraft configuration with multiple fast actuated control surfaces are introduced. The modeling approach, developed at the Institute of Aircraft Systems Engineering (FST) of the Hamburg University of Technology (TUHH), as well as the required CFD data generation, conducted by the Institute of Aerodynamics and Gas Dynamics (IAG) of the University of Stuttgart, are presented in section 3. In section 4, the proposed model is analyzed with regard to the achieved accuracy compared to the CFD data and its overall suitability within efficient flight dynamics analysis.

2. FLIGHT DYNAMICS BASE MODEL

In this paper, the here proposed method for the efficient modeling of unsteady control surface aerodynamics is demonstrated for an aircraft configuration with a multi-control surface intelligent wing design. Therefore, the reference aircraft and its flight dynamics base model are presented in the following.

2.1. Reference Aircraft

The demonstration of the control surface model is done using a medium-range commercial airliner configuration. The reference aircraft is a modification of the DLR LEISA configuration, initially generated for the LuFo Project LEISA by the DLR [4]. In the LuFo Projects Polamin and INTELWI, the configuration was upgraded with trailing edge tabs (TET) and dynamic droop nose leading edge flaps (DN), capable of fast deflection in cruise conditions [5] [6]. The all-speed TETs are located within the low-speed-only Fowler flap. In total, there are 5 DNs and 4 TETs in addition to the classical aileron, such that almost the whole leading and trailing edges are equipped with fast movables. The Tab layout can be seen in figure 3. All tabs and the aileron can be used for loads control, as published by Ullah et al. [5] [7]. In this work, TET 1 and TET 2 are treated as one single control surface. The same applies to DN 1 and DN 2. Thereby, the reference configuration has 16 dynamic control surfaces at the wing: 4 individual DNs, 3 individual TETs and one Aileron.

2.2. Model structure

The flight dynamics base model, developed at the TUHH, is implemented in MATLAB/Simulink and consists of several sub models for the various model domains, as depicted in figure 1. Therefore, the inhouse model library *FlySim* is utilized, which offers different levels of model accuracy and thereby model complexity for various model domains.
Main part of the model are the equations of motion to simulate the aircraft motion, taking into account all 6 degrees of freedom of the rigid body motion. Inputs to the equations of motion are the forces and moments resulting from the aerodynamics, inertia, gravity and engines. In addition to the rigid body motion, the structural dynamics are accounted for by a modal model determining the deformation from a stability axis coordinate system. Hence, the actual aerodynamic forces are calculated as a result of the aeroelastic coupling. Both, in order to couple the aerodynamic model with the structural dynamics model and in order to calculate structural loads at various span stations of the wing, the calculation of distributed aerodynamic forces and moments is necessary. Therefore, the aircraft is divided into 132 chordwise stripes, for which the aerodynamic forces and moments are calculated individually, as schematically depicted in figure 2. One of these stripes represents the tail surfaces, i.e. the horizontal tailplane and the vertical tailplane. Another stripe represents the fuselage and the remaining 130 stripes together represent the main wings. For each stripe, the set of the three aerodynamic forces lift, drag and sideforce as well as the three aerodynamic moments, roll-, pitch- and yaw-moment, is calculated by interpolation of lookup tables of aerodynamic coefficients and derivatives, identified from CFD data. For the calculation, the local free stream velocity, its angles to the mean body axis as well as the local deformation angles, e.g. the local twist deformation due to elasticity, of the respective stripe are considered.
The most important aircraft systems, when investigating the aircraft behavior during wind gust encounters and extreme maneuvers, are the engines, the actuation system and the flight control system. For the engines model, the maximum available thrust is determined by lookup tables as a function of the current altitude and mach number. This maximum value is then scaled with the current thrust lever position, ranging from 0 to 1. The dynamics of the engine spool-up and spool-down are not yet implemented but in order to avoid unrealistically fast thrust changes, the thrust rate of change is limited by the thrust controller.
The actuation system for the dynamic control surfaces of the *Intelligent Wing* is a central aspect of current re-

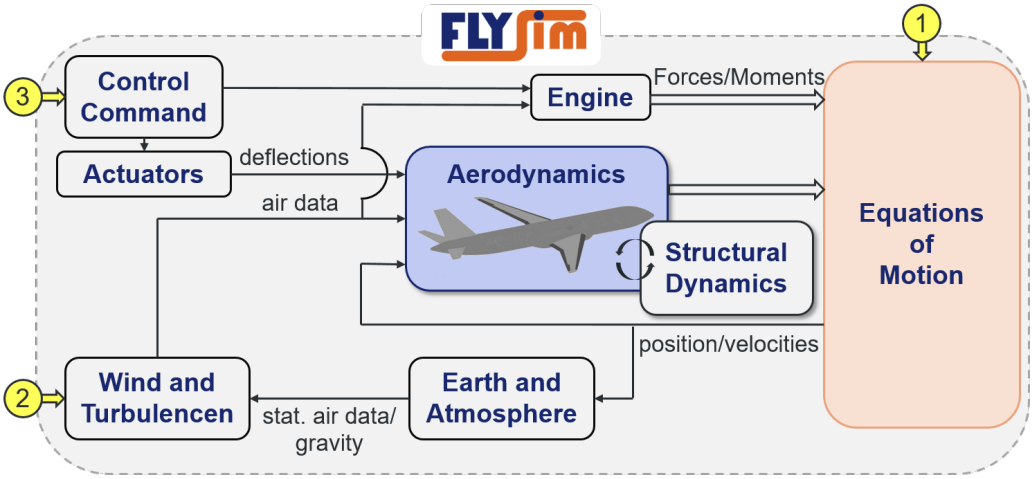

FIG 1. Main components of the flight dynamics base model

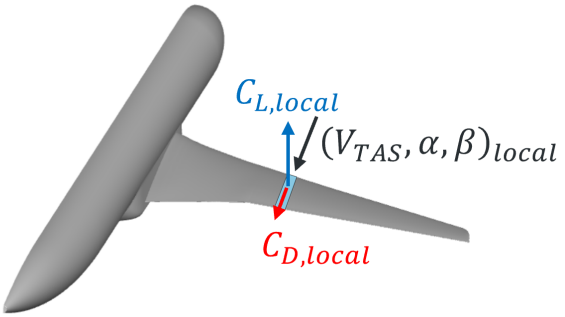

FIG 2. Schematic depiction of the local lift and drag calculation of a wing stripe

search at the TUHH. It's design is an iterative process and the effect of design decisions can influence the flight dynamically relevant control functions. Hence, in this model, the actuation system can be run as a co-simulation with the newest models from actuator design. Thereby, the actuator dynamics within the flight dynamics model are easily adapted to the most recent state of design.

For the flight control system, an industry-like cascade control is implemented, based on the descriptions in [8]. The control loops are cascaded according to their control dynamics from the fastest innermost damping loop to the slowest outermost position control loop. The individual controller gains are scheduled for the variables altitude and airspeed in order to achieve good control behavior within the full flight envelope. The flight control system includes a manual flight mode with the rudder pedals and sidestick inputs as interfaces. They can either be controlled by the user during the simulation or by a preset signal to simulate preplanned maneuver scenarios. Different autopilot modes are included, controlling the altitude and heading, the pitch and roll attitude or the sinkrate and sideslip angle. This basic flight controller shall be expanded with additional control functions as load control.

The environmental model is divided into the *Earth and Atmosphere* model and the *Wind and Turbulence* model. The *Earth and Atmosphere* model determines the static air data at the current flight altitude, as air pressure, temperature and density according to the International Standard Atmosphere (ISA) [9] with the additional option for temperature differences. Furthermore, it determines the local earth gravitational field and the local magnetic field using the definitions of WGS84 [10] and EGM96 [11]. The *Wind and Turbulence* model is used to simulate the following specified wind scenarios:

- Constant horizontal wind from an arbitrary direction
- Discrete wind gusts with 1-cos shape, as defined by the certification specification *CS-25* for large aeroplanes [12]
- Wind shear
- Stochastic turbulence fields according to the military standard *MIL-F-8785C* [13]

For management and control of the simulations, three interfaces are provided to the user, marked by the yellow circles in figure 1. As the first input, the user can select the initial conditions for the equations of motion by selection of an arbitrary trim point. This determines the initial position, attitude and velocity of the aircraft, as well as the initial position of all control surfaces. As the second input, the user can select which wind or turbulence scenarios will occur during the simulation. Both, the magnitude and the start time of the wind scenario can be chosen. Finally, the user can select one of the above mentioned controller modes of the flight control system. An interaction with the flight control system is also possible while the simulation is running.

3. EFFICIENT UNSTEADY CONTROL SURFACE MODEL

In the following, the efficient modeling of unsteady aerodynamic effects of dynamically deflected control surfaces in the transonic flight regime is presented. The model is exemplary generated for the reference

aircraft, presented in section 2.1. First, the generation of the aerodynamic data set via CFD calculations for the model development and its subsequent evaluation is described in section 3.1. In section 3.2, the general model structure of the efficient reduced order model (ROM) is introduced. Thereafter, the optimization of the arising design variables of the model is discussed in section 3.3.

3.1. CFD calculations for the aerodynamic data set

The grid and main setup used for the CFD simulations within this work are equivalent to the one of Ullah et al. presented in [7]. It is briefly summarized here to provide a stand-alone understanding of the work at hand. Further details on the CFD setup and the underlying methods, i.e. for flap deflection, can be found in [7]. Unsteady Reynolds-averaged Navier-Stokes (RANS) simulations were performed for the aerodynamic CFD dataset with steady and unsteady flap deflections. Therefore, the unstructured, finitevolume DLR TAU solver [14] was used. The RANS equations are closed by utilizing the Spalart- Allmaras turbulence model in its original form. All CFD simulations were performed at $H = 35\,000\,\mathrm{ft}$, $M = 0.8$ and $C_L = 0.5$ for the wing-fuselage configuration shown in Fig. 2. The flap deflection is realized via grid deformation based on radial-basis functions, see [7]. The time function of the flap deflection $\delta(t)$ is based on a gust encounter scenario, identified as critical for the current flight case in [7] with a critical gust wavelength $\lambda = 50\,\mathrm{m}$. The flaps are deflected similar to the 1-cos function of the critical gust shape as used for gust load alleviation, see [7]. The corresponding flap deflection function is defined to

$$\delta(t) = \frac{\delta_{max}}{2} \cdot \left[1 - \cos\left(\frac{2 \cdot \pi \cdot t}{T}\right)\right] \tag{1}$$

with

$$T = \lambda / U_\infty \tag{2}$$

Two different deflection types are used within this work. In case a full deflection and retraction cycle is simulated, the function is applied for $0 <= T$. The second case is a full deflection up to δ_{max}, with the flap not being retracted, but held in this position. Hence, the flap deflection function is applied for $0 <= T/2$ with $\delta(t) = \delta_{max}$ for $t > T/2$. In line with Ullah et al. [7], the time step size is selected to $T/150$ with 400 inner iterations at each time step.

3.2. Control surface model structure

In accordance with the method published by Lancelot et al. [3], the total aerodynamic effect ΔQ_c of the control surface at dynamic deflection is divided into a steady portion ΔQ_{cs} and an unsteady portion ΔQ_{cu}, following equation 3.

$$\Delta Q_c = \Delta Q_{cs} + \Delta Q_{cu} \tag{3}$$

The steady portion represents the deviation of the aerodynamic coefficient from the clean wing, which would be reached when the current surface angle is held constant over a long time span. The unsteady portion is determined by the intermittent difference from the total effect and the steady effect during a dynamic change in deflection angle.
Lookup tables are used for mapping the current deflection angle at the current flight point, i.e. altitude and airspeed, to the steady aerodynamic effect. For the unsteady effect, transfer functions are used with the deflection rate as input signal.
Theoretically, a control surface deflection has an effect on all six aerodynamic coefficients (lift, drag, sideforce, pitch-, roll- and yaw-moment) at each aircraft stripe of the stripe model introduced in section 2.2. For the here considered reference aircraft with 16 dynamic control surfaces and a discretization of the aerodynamic model using 132 stripes, this leads to a total of 12,576 transfer functions plus 96 lookup tables. The modeling effort as well as the computation effort for this high number of individual transfer functions is significantly too large for the fast comparison and evaluation of different load control functions. Hence, a further improvement especially of the unsteady model part is discussed in the following.
The first simplifying assumption is that each control surface only affects the wing side at which it is positioned, e.g. the right aileron only effects the aerodynamic coefficients of the right wing stripes. Thereby, the required number of transfer functions and lookup tables can already be cut in half.
For the second simplification, the wing is divided into a few spanwise wing sections. For the here considered reference aircraft, 7 wing sections are chosen, as depicted in figure 3 and discussed in section 3.3.1.

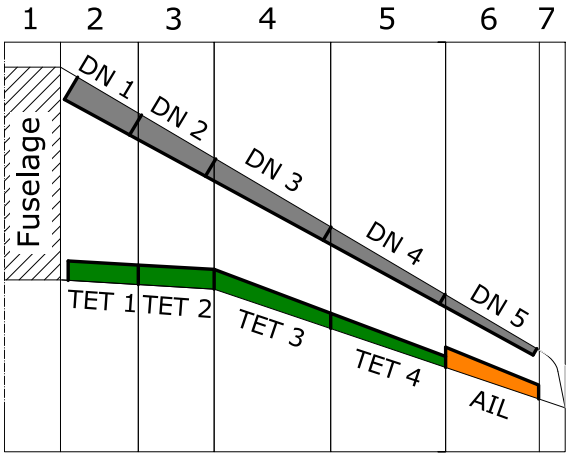

FIG 3. Location of the trailing edge tabs (TET), droop nose (DN), Aileron (AIL) and wing sections for the reduced unsteady aerodynamics model

For each wing section, the spanwise distribution of the unsteady effect is determined at a time stamp

t_x and saved within a lookup table. This distribution is then scaled over the time by one single transfer function, identified by the unsteady effect at the span position WS_y, as depicted in figure 4. Thereby, the number of transfer functions is reduced by the factor $k \approx 9$ according to equation 4 with $n_{sections} = 7$ and $n_{stripes} = 65$ per wing.

$$k = \frac{n_{stripes}}{n_{sections}} \tag{4}$$

Just like Lancelot et al. proposed, the transfer functions are estimated from single CFD analysis data for a dynamic deflection of the control surface using the MATLAB function *tfest* [15]. Thereby, the number of poles and zeros of the transfer functions must be selected in advance. As this is a trade-off between the transfer function complexity and the accuracy, an optimization is possible and will be conducted in the following.

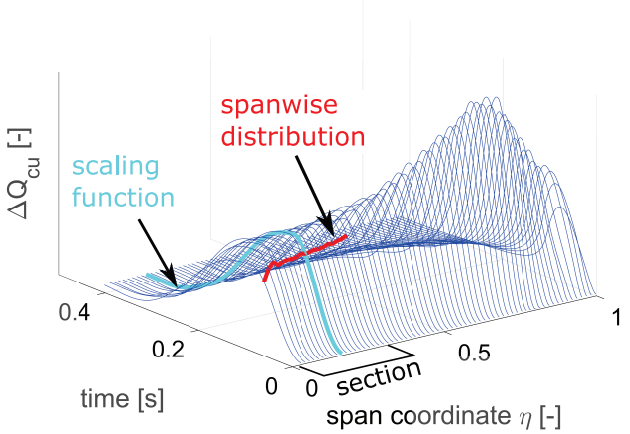

FIG 4. Example selection of a spanwise distribution vector and a scaling function for the unsteady effect of an aileron deflection at Mach 0.8

3.3. Optimization of design variables

In total, the following design variables need to be chosen optimally during the identification of the control surface model:

1) Number of wing sections and the location of their cuts
2) Selection of the span position WS_y at which the transfer function is identified
3) Selection of the transfer function order, i.e. the number of poles and zeros
4) Selection of the time stamp t_x at which the distribution of the unsteady effect is taken

The determination of these design variables is discussed in the following. In order to evaluate the optimization results, an error is formulated according to equation 5.

$$E_{sq} = \sum_{\eta_{section}} \sum_{t} \left(\Delta Q_{c,ROM} - \Delta Q_{c,CFD}\right)^2 \tag{5}$$

Here, the deviation of the unsteady model prediction $\Delta Q_{cu,ROM}$ from the CFD calculation $\Delta Q_{cu,CFD}$ is summed up for each time step t and each span position $\eta_{section}$. This leads to a single numerical value giving a summary of the overall fit of the reduced order model.

3.3.1. Determination of the wing sections

As only one transfer function is assigned to each wing section to scale the distribution of the unsteady effect, the transient behavior of the whole section is uniform. Hence, areas with significantly different transient behavior need separate wing sections. In figure 5 it can be seen, that the transient behavior changes significantly across the wing span. In this example, the maximum unsteady effect at the aileron itself is reached after approximately $0.08\,\mathrm{s}$ and significantly falls again until $0.15\,\mathrm{s}$, as can be seen by the plot of $\eta = 0.7$. In relation to this, the transient behavior of the unsteady effect outside of the control surface is slower. Especially after the control surface has stopped, the reduction of the unsteady effect is significantly delayed close to the wing root, as can be seen by the plot of $\eta = 0.03$. Thereby, a single transfer function for the whole wing to scale a full-span effect distribution would lead to a significant inaccuracy. The actual number of sections is a trade-off between the overall accuracy and the model complexity. As a first assumption, the wing sections were cut in alignment with the tab cuts, i.e. each wing section covers the wing span portion of one trailing edge tab. Additionally, the fuselage needs an individual section, as its transient behavior significantly differs from that of the wing stripes. Finally, for the wing tip a separated section was implemented as well, in order to refine the accuracy in this area. The unsteady effect of a dynamic aileron deflection on the wing stripes of each wing section can be seen in figure 6.

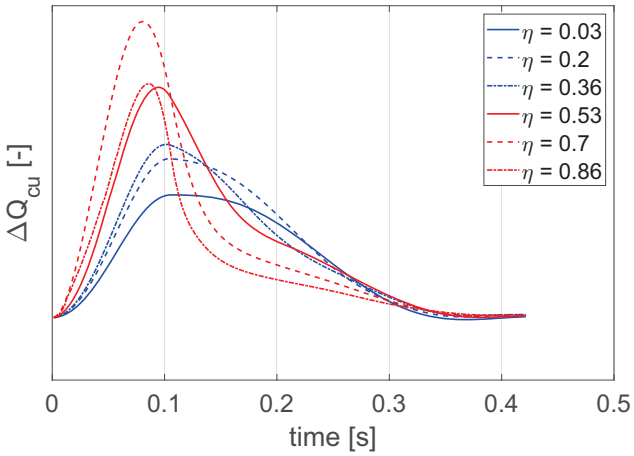

FIG 5. Unsteady effect of a dynamic aileron deflection at Mach 0.8 on wing stripes at different span positions

3.3.2. Selection of the span position at which the transfer function is identified

It was found, that the span position at which the transfer function is identified only has a minor effect on the overall accuracy of the reduced order model. In some cases, when the considered wing section was not in the vicinity of the deflected control surface, there was no influence on the accuracy at all.
Nevertheless, a global optimization of the variable was included into a multivariable optimization procedure. In this procedure, the relevant parameters, WS_y, the transfer function order and t_x, are varied over their full range. The transfer functions are calculated individually for each control surface and for the whole grid generated by the parameter variation. For all transfer functions, a comparison with the CFD data set is conducted in form of the squares error determination according to equation 5. Finally, the best combination of parameters can be determined by the lowest square error. This procedure is used as the effect of the parameter variation does lead to many local minima, which makes it complicated for gradient based optimization algorithms to find the global minimum. In all cases where the span position for the transfer function identification has no influence on the model accuracy, the mid span position of the considered wing section is used.
Exemplary, figure 6 shows the selected transient data set of each wing section for transfer function identification of the aileron deflection, marked with the red line. All other transient data sets of the remaining stripes of the wing section are marked with gray lines for comparison.

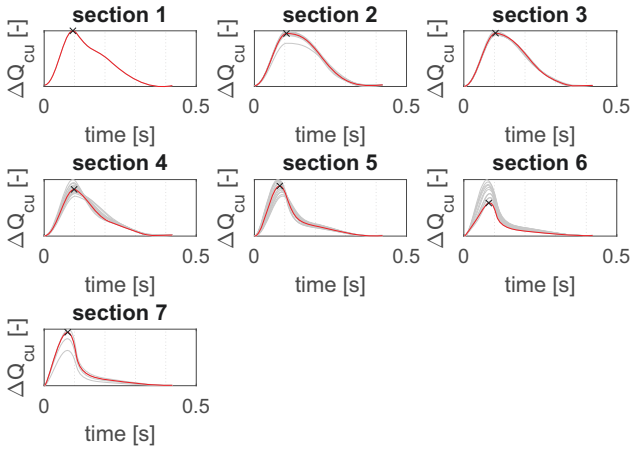

FIG 6. Unsteady effect of a dynamic aileron deflection at Mach 0.8 on the wing stripes sorted by sections; red line: chosen wing stripe for transfer function identification; black cross: time stamp at which the distribution vector is determined; gray lines: transient data sets of all stripes within the wing section

3.3.3. Selection of the transfer function order

A higher number of poles and zeros of the transfer function enable the modeling of a more complex transient behavior. However, the computation demand also rises with the order of the transfer functions. Similar to the recommendation of Lancelot et al. [3], it was found that a maximum of four to five poles and zeros lead to a good fit of the estimated transfer functions with the predetermined data set. The fit of the transfer functions is determined by the MATLAB function *tfest* in form of the fit percentage according to equation 6 [16].

(6)
$$FitPercent = 100 \cdot \left(1 - \frac{||y_{measured} - y_{model}||}{||y_{measured} - \overline{y_{measured}}||}\right)$$

Here, $y_{measured}$ is the measured output data, i.e. the actual CFD data the transfer function should predict. $\overline{y_{measured}}$ is the mean of the measured data and y_{model} is the predicted data of the transfer function. With some exceptions, most estimated transfer functions achieve a fit percentage of 90 or more. In all other cases the lower fit percentage was accepted, as the overall result for the wing section produces a good result, as can be seen from low squared error values E_q, see equation 5.
The actual number of poles in each transfer function is determined individually by the optimization procedure introduced in section 3.3.2. The number varies between 2 and 5 in most cases.

3.3.4. Selection of the time stamp at which the distribution of the unsteady effect is taken

As can be seen from figure 5, the maximum unsteady effect is reached at different times for different span positions. This implies, that the best time stamp t_x to identify the unsteady effect distribution vector may be different for each section. Additionally, t_x can also vary for each control surface deflection. Hence, an optimization for each wing section and control surface is necessary.
t_x is varied over the full time range of the training signal of $0.43\,\mathrm{s}$ in 300 steps in the optimization procedure introduced in section 3.3.2 to find the best combination of t_x and WS_y.
As can be seen in the example of the aileron deflection in figure 6, as expected the distribution vector of the unsteady effect is automatically taken at the vicinity of the peak of the unsteady effect, as indicated by the black cross.

4. ANALYSIS

In the following, the proposed efficient modeling of unsteady control surface aerodynamics is analyzed and evaluated. Firstly, the superposition procedure, where the effect of an arbitrary combination of control surface deflections is predicted by superposition of the effects of isolated control surface deflections, is analyzed in section 4.1. Thereafter, the achieved model accuracy is analyzed by evaluation of the reduced order model results for the total transient effect of iso-

lated tab deflections and by their spanwise distributed effects in section 4.2 and for combined tab deflections in section 4.3.

4.1. Analysis of the superposition procedure for combined control surface deflections

The here proposed modeling strategy for the unsteady aerodynamic effect of arbitrary tab deflections utilizes the isolated models for each individual tab and the subsequent superposition of their results. Hence, at this point, it is shortly demonstrated, that the superposition method leads to an acceptable accuracy for combined tab deflections. In figure 7, a comparison of a CFD analysis of a combined upwards deflection of all trailing edge tabs with the superposition of CFD results from the isolated trailing edge tabs deflected in the same angle is shown. The comparison is made for the three most relevant coefficients with respect to loads control: the lift coefficient, as it is primarily responsible for the wing bending moment, the pitching moment coefficient, as it is primarily responsible for the wing torsional moment and the drag coefficient, as it is primarily responsible for cruise performance degradation and passenger discomfort when changed dynamically.
As can be seen in figure 7, the superposition procedure leads to very similar effects, compared to the analysis of the combined deflection, with a maximum error of $3.6\,\%$ and $4.5\,\%$ of the maximum effect for the lift and the pitching moment coefficients, respectively. Only regarding the drag coefficient, some small deviations are visible with a maximum error of $9.3\,\%$ of the maximum effect.

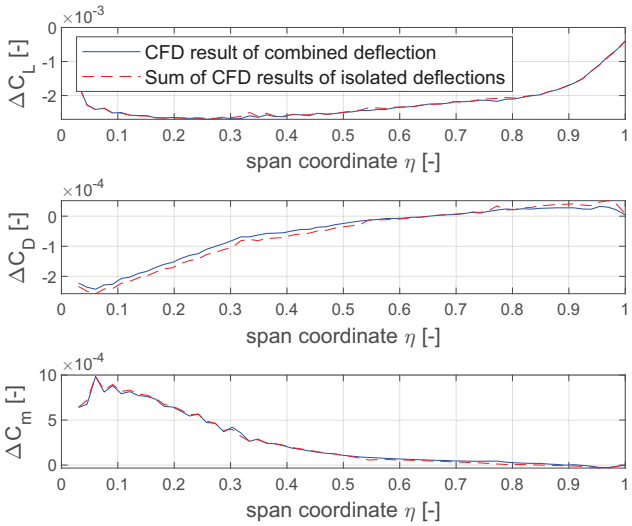

FIG 7. Comparison of the superposition procedure with CFD results for the total effect of all trailing edge tabs deflected upwards simultaneously at Mach 0.8

4.2. Analysis of ROM results for isolated tab deflections

In order to demonstrate the accuracy of the proposed ROM for isolated control surface and tab deflections, their predictions are compared with CFD data in this section. First, the total effect on the aircraft forces and moments coefficients are analyzed. Figures 8 and 9 show the comparison of those total effects for the deflection of all trailing edge tabs and droop noses individually. In this paper, the analysis is limited to the lift, drag and pitching moment coefficient, as they have the most relevant effect on load control functions, see section 4.1.
In general, the dynamic trailing edge tab deflections have a significant effect on all three of the considered coefficients. Hence, they are suitable for the reduction of the design wing bending moment by adjusting the total lift and its spanwise distribution during maneuvers and gust encounters. However, this will induce unwanted pitching moments and thereby increases the wing torsional moment [7] [17]. And lastly, by effecting the drag coefficient, the passenger comfort and the cruise performance in turbulent air have to be investigated cautiously.
In the following, an error formulation according to equation 7 is used for evaluation, where the total error is taken relative to the maximum value of the target CFD data of the considered tab.

$$E_{rel} = \frac{\Delta C_{i,ROM} - \Delta C_{i,CFD}}{max(|\Delta C_{i,CFD}|)} \tag{7}$$

For the trailing edge tabs, the highest measured relative error at lift coefficient calculation is $1.7\,\%$ at TET 5. The pitching moment is similarly well predicted with a maximum relative error of $3.0\,\%$ at TET 4. The drag coefficient shows a more complex transient behavior, especially for deflections of tabs 3 to 5. Thereby, the highest measured relative error at drag coefficient calculation is $8.3\,\%$ at TET 4. Nevertheless, the model accuracy regarding the effect of the tab's drag coefficient on the total aircraft drag is acceptable, as the higher relative errors occur only at the outer tab, where the absolute aerodynamic effect is comparably low. Thereby, the absolute drag error at TET 4 and TET 1+2 are almost identical at around $5.3 \cdot 10^{-5}$, although TET 1+2 has a relative drag error of only $1.7\,\%$.
In general, the droop nose deflections have a minor effect on the lift coefficient but a significant effect on the pitching moment and the drag coefficient. Hence, they may be used in combination with trailing edge tabs for load control functions to compensate the wing torsional moment induced by the TET deflections, as described e.g. by Ullah et al. [5].
For the droop noses, the highest measured relative error at lift coefficient calculation is quite high with $55.3\,\%$ at DN 3. This is a result of a delayed reaction of the ROM model to the control surface deflection due to slightly inaccurate transfer function identifications. In general, the lift coefficient prediction is less

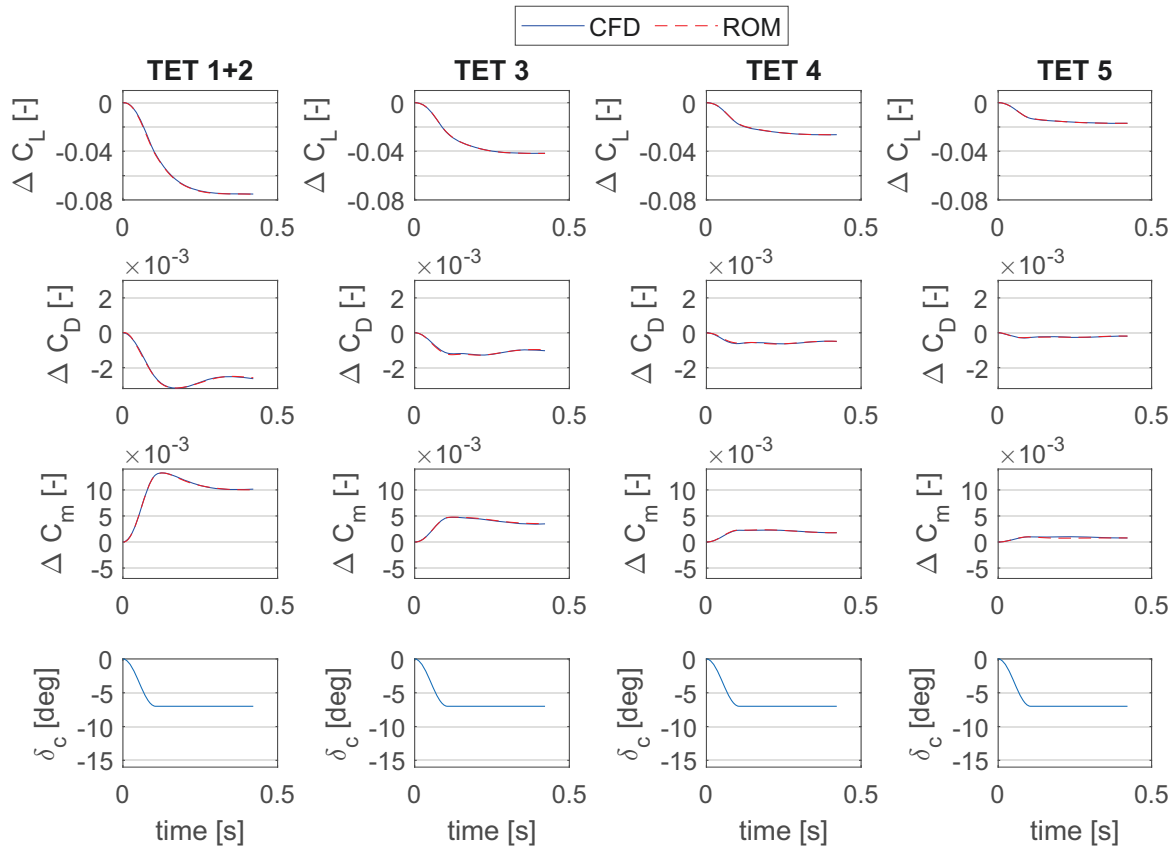

FIG 8. Comparison of the ROM with CFD data for the total lift, drag and pitching moment coefficient effect of trailing edge tab (TET) deflections at Mach 0.8

accurate for the droop noses. Main reason is the more complex transient behavior compared to that of a trailing edge tab deflection. As the droop nose deflection has a small effect on the lift in general, these higher errors are accepted. The accuracy of the ROM prediction for the pitching moment coefficient and the drag coefficient are again comparable to that of the trailing edge tabs. The maximum relative error at pitching moment prediction is $2.9\,\%$ at DN 4 and the maximum relative error at drag prediction is $8.2\,\%$ at DN 3.

In the following, the spanwise distribution of the above mentioned effects is analyzed for the examples of the pitching moment and the drag, as they are the main effects of a droop nose deflection. Figure 10 shows the distributed pitching moment coefficient effect of an aileron / TET 5 deflection at Mach 0.8. The deflection signal is the same, as in figure 9. Interesting to notice is that the effect is increasingly delayed with spanwise distance to the control surface. Although this gradual increase in delay is approximated by a few wing sections, each with a single transfer function, the results match up with the CFD data qualitatively good. Only at some spots, light deviations of the ROM predictions from the CFD data are visible. But these deviations are not expected to have a significant influence on the planned flight dynamical simulations.

Figure 11 shows the distributed drag coefficient effect of a dynamic deflection of DN 4 at Mach 0.8. The deflection signal again is the same, as in figure 9. Here, the more complex transient behavior of the various wing span positions can be seen. While the drag at the span position of DN 4 immediately decreases for some milliseconds at the start of the deflection, it is initially mostly constant for span sections further away from the tab. After this initial decrease, the drag at the tab rises rapidly with a slight overshoot of the steady effect, building thereafter. A comparable behavior can be seen for the rest of the wing span, but for the span section between $\eta = 0.2$ and $\eta = 0.55$, a noticeable second overshoot can be seen. All in all, the ROM follows all these effects quite well. Some noticeable deviations occur at a few wing stripes at the initial drag decrease and the subsequent overshoot at the tab itself. This is due to the simplification made by the sectioning procedure of the unsteady effect and thereby shows the trade-off between accuracy and model complexity.

4.3. Analysis of ROM results for combined tab deflections

After the overlay procedure has been demonstrated based on CFD data only in section 4.1 and the efficient unsteady aerodynamics model was analyzed for isolated tab deflections in section 4.2, in this section the combination of both is analyzed. Therefore, the ROM-predicted unsteady aerodynamic effect of a combined deflection of tabs is compared to CFD data. Figure 12 exemplary shows the lift effect of a combined dynamic deflection of all trailing edge tabs from $0°$ to $-10°$ within approximately $0.2\,\mathrm{s}$ at Mach 0.8. As

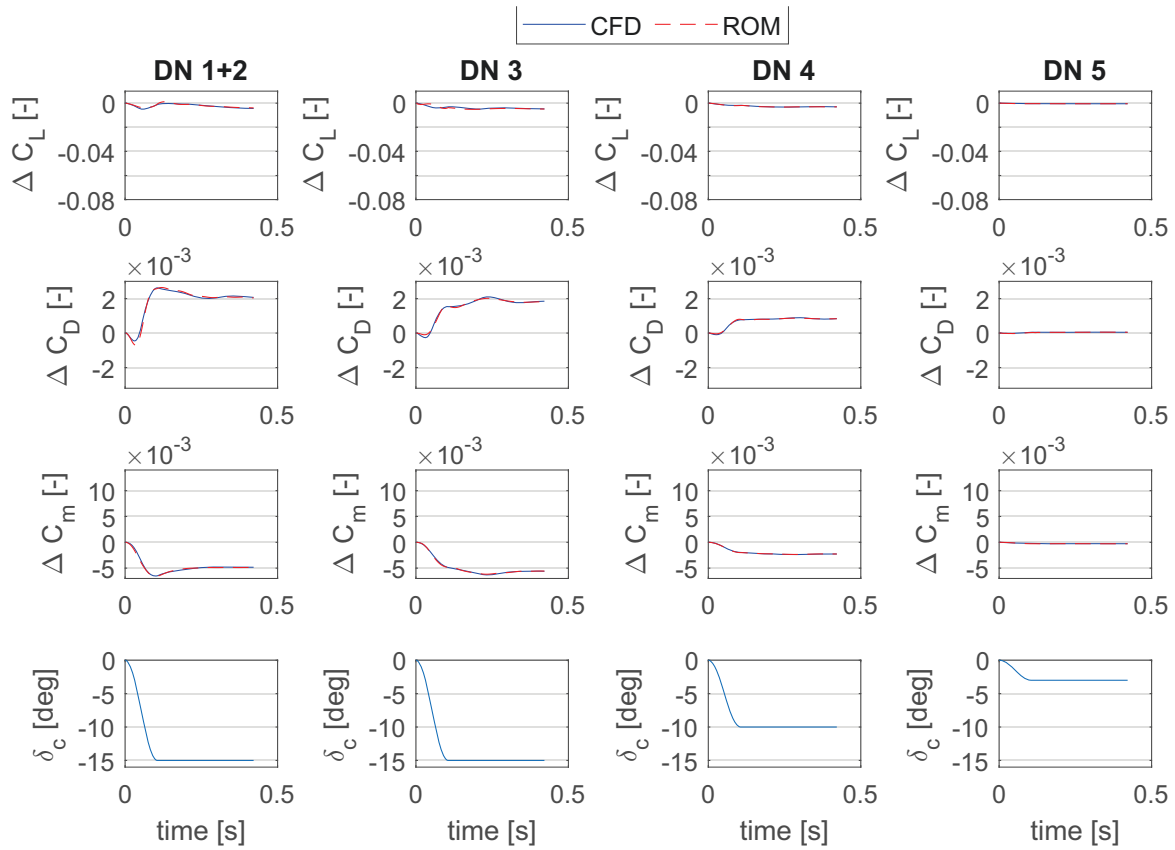

FIG 9. Comparison of the ROM with CFD data for the total lift, drag and pitching moment coefficient effect of droop nose (DN) deflections at Mach 0.8

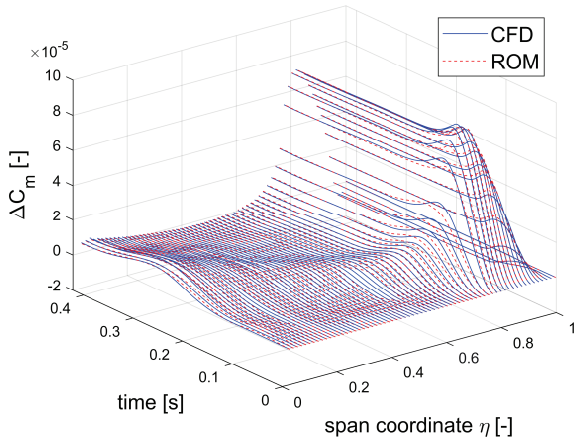

FIG 10. Comparison of the ROM with CFD data for the distributed pitching moment coefficient effect of a dynamic aileron deflection at Mach 0.8

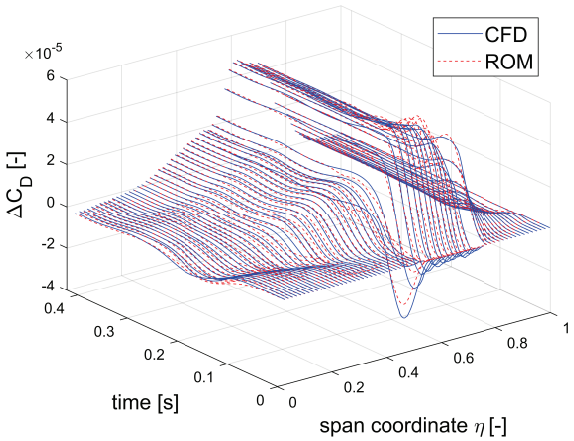

FIG 11. Comparison of the ROM with CFD data for the distributed drag coefficient effect of a dynamic deflection of DN 4 at Mach 0.8

can be seen, both, the transient behavior of the lift effect as well as its spanwise distribution are predicted quite satisfactorily.

As expected, for the further coefficients, the accuracy is also acceptably high, following the same minor issues already discussed for the superposition procedure in section 4.1 and the general prediction of more complex transient behavior e.g. at the drag coefficient, as discussed in section 4.2. To conclude these analysis, the obtained relative errors for the current example of a combined dynamic deflection of tabs are calculated. Therefore, the error definition in equation 7 is used. With this definition, the maximum error for each wing stripe is calculated. As the approach of sectionizing the wing will inevitably result in larger errors of single wing stripes, an additional mean error $\overline{E}_{rel}$ needs to be defined in order to evaluate the overall accuracy. This is done according to equation 8.

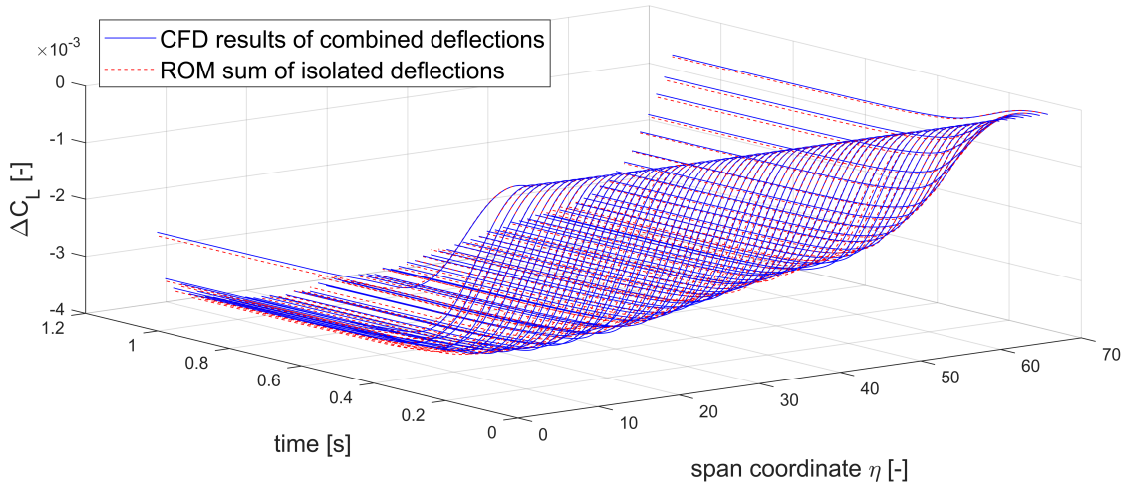

FIG 12. Comparison of the ROM with CFD data for the distributed lift coefficient effect of a combined dynamic deflection of all trailing edge tabs at Mach 0.8

$$\overline{E}_{rel} = \frac{\sum_{i=1}^{n_{str}} E_{rel,i}}{n_{str}} \tag{8}$$

The achieved results are summarized in table 1. As can be seen, the highest measured relative error at lift effect prediction is only $1.14\,\%$ and the mean error is even lower at $0.30\,\%$, which demonstrates the good functionality of the proposed procedure for flight mechanical analysis including load reduction functions targeting the wing bending moment. Although the maximum relative error at pitching moment prediction is quite high with $15.7\,\%$, the mean relative error is acceptable low at $2.86\,\%$ because the high errors are only present at few wing stripes. Thereby, the proposed procedure is also suitable for monitoring the wing torsional moment at flight mechanical analysis including load reduction functions. Lastly, the errors for the drag effect prediction are also acceptably low, which also enables the monitoring of the load alleviation function's influence on cruise performance and passenger comfort.

coefficient	highest E_{rel}	$\overline{E}_{rel}$
ΔC_L	$1.14\,\%$	$0.30\,\%$
ΔC_D	$6.24\,\%$	$1.56\,\%$
ΔC_m	$15.7\,\%$	$2.86\,\%$

TAB 1. Maximum relative error and mean relative error of ROM predictions for a combined dynamic deflection of all trailing edge tabs at Mach 0.8

5. CONCLUSIONS

In this paper, an efficient modeling approach for the unsteady aerodynamic effect of tabs or control surface deflections is presented. The model uses data from stationary CFD analysis to generate lookup tables for the steady effect prediction of each isolated control surface deflection and data from selected unsteady CFD analysis to identify transfer functions for the additional unsteady effect. Hereby, the transfer function scales a spanwise distribution vector of the unsteady effect for a wing section. By selecting the number of sections the wing is divided into, the compromise between complexity and accuracy can be adjusted. For the here considered wing with multiple movables covering almost the complete leading and trailing edges of the wing, a coincidence of the tab cuts and the section cuts lead to feasible results. Further design parameters at the identification process of the unsteady effect are the selection of the span position WS_y, at which the transfer function is identified, the order of the transfer functions and the selection of the time stamp t_x, at which the distribution of the unsteady effect is taken. In this paper, the optimization of those parameters is demonstrated. It was found, that in most cases the span position WS_y has almost no influence on the model accuracy. Furthermore, the best time stamp t_x is at the time of maximum unsteady effect in most cases and a transfer function order of 4 to 5 leads to reasonably good results.
The effect of an arbitrary combination of tab deflections is calculated by superposition of the predicted effects due to the isolated deflection of each tab. Using an example with all trailing edge tabs deflected simultaneously, it was shown that the proposed modeling strategy leads to an quite accurate unsteady control surface aerodynamics model. The mean relative errors for this example were shown to be less than $3\,\%$ for the most important aerodynamic coefficients at investigation of load control functions.
In total, the model is sufficiently accurate and acceptably fast for the integration into a flight dynamics model with the goal of simulating a broad spectrum of maneuvers and gust encounters for controller and systems evaluation.

Acknowledgments:

The authors would like to thank Christian Breitenstein of the Institute of Fluid Mechanics of the Technical University of Braunschweig for the development and supply of an extensive CFD data base required for the base flight dynamics model of the reference aircraft configuration.
This work was founded by the German Federal Ministry for Economic Affairs and Climate Action within the project INTELWI in the national LuFo program (contract codes 20A1903K and 20A1903B). Their support is greatly appreciated.

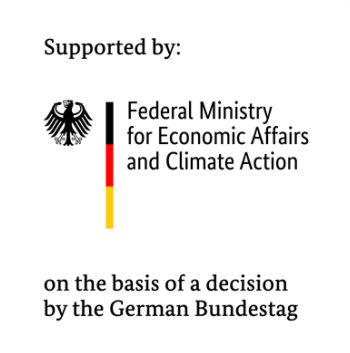

Contact address:

lars-hendrik.lemke@tuhh.de

References

[1] K. M. Roughen, M. L. Baker, and T. Fogarty. Cfd and doublet-lattice calculation of unsteady control surface aerodynamics and correlation with wind tunnel test. 1999.

[2] Thiemo Kier. Comparison of unsteady aerodynamic modelling methodologies with respect to flight loads analysis. 2012. DOI: 10.2514/6.2005-6027.

[3] Paul Lancelot and Roeland De Breuker. Unsteady non-linear control surface modelling for aeroservoelastic applications. *ASDJournal*, 2020(8), 2021. DOI: 10.3293/asdj.2020.56.

[4] Jochen Wild, Michael Pott-Pollenske, and Björn Nagel. An integrated design approach for low noise exposing high-lift devices. *3rd AIAA Flow Control Conference*, 2006.

[5] Junaid Ullah, Thorsten Lutz, Lorenz Klug, Rolf Radespiel, and Jochen Wild. Active gust load alleviation by combined actuation of trailing edge and leading edge flap at transonic speeds. *AIAA SciTech Forum*, 2021. DOI: 10.2514/6.2021-1831.

[6] Marco Hillebrand, Jens Müller, Junaid Ullah, and Thorsten Lutz. Investigation of a realistic flap modeling using a combination of chimera method and grid deformation on a wing fuselage configuration. *PAMM*, 22(1), 2023. ISSN: 1617-7061. DOI: 10.1002/pamm.202200101.

[7] Junaid Ullah, Thorsten Lutz, Lorenz Klug, Rolf Radespiel, Jochen Wild, and Ralf Heinrich. Approach for aerodynamic gust load alleviation by means of spanwise-segmented flaps. *Journal of Aircraft*, 60(3):835–856, 2023. ISSN: 0021-8669. DOI: 10.2514/1.C037086.

[8] Rudolf Brockhaus, Wolfgang Alles, and Robert Luckner. *Flugregelung*. Springer Berlin Heidelberg, Berlin, Heidelberg, 2011. DOI: 10.1007/978-3-642-01443-7.

[9] U.S. Government. U.s. standard atmosphere, 1962, 1963.

[10] National Imagery and Mapping Agency. Nima tr8350.2 - department of defense world geodetic system 1984, 2000.

[11] F.G Lemoine, S. C. Kenyon, J.K Factor, R. G. Trimmer, N. K. Pavlis, D. S. Chinn, C. M. Cox, S. M. Klosko, S. B. Lutcke, M. H. Torrence, Y. M. Wang, R. G. Williamson, E. C. Pavlis, R. H. Rapp, and T. R. Olson. The development of the joint nasa gsfc and the national imagery and mapping agency (nima) geopotential model egm96, 1998.

[12] European Union Aviation Safety Agency. Certification specifications and acceptable means of compliance for large aeroplanes cs-25: Amendment 26, 2019.

[13] U.S. Department of the Air Force. Military specification - flying qualities of piloted airplanes (mil-f-8785c), 1969.

[14] Dieter Schwamborn, Thomas Gerhold, and Ralf Heinrich. The dlr tau-code: Recent applications in research and industry, 2006.

[15] tfest: Estimate transfer function model. https://de.mathworks.com/help/ident/ref/tfest.html.

[16] Loss function and model quality metrices. https://de.mathworks.com/help/ident/ug/model-quality-metrics.html.

[17] Christian Breitenstein, Jens Müller, Marco Hillebrand, Malte Woidt, Matthias Haupt, and Rolf Radespiel. Fluid-structure coupled analysis of maneuver load alleviation on a large transport aircraft. *AIAA AVIATION 2023 Forum*, 2023. DOI: 10.2514/6.2023-3953.